Urban Climate 52 (2023) 101735

Contents lists available at ScienceDirect

Urban Climate

journal homepage: www.elsevier.com/locate/uclim

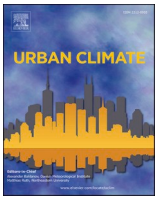

Effect of heatwaves on urban sea breeze, heat island intensity, and outdoor thermo-hygrometric comfort in Rome (Italy)

Annalisa Di Bernardino [a,*], Serena Falasca [a], Anna Maria Iannarelli [b], Stefano Casadio [b], Anna Maria Siani [a]

[a] Physics Department, Sapienza University of Rome, Rome 00185, Italy
[b] SERCO Italia SpA, Frascati, Rome 00044, Italy

ARTICLE INFO

Keywords:
Extreme heat events
Urban areas
Climate change
Urban heat island
Thermo-hygrometric comfort
Coastal meteorology

ABSTRACT

The purpose of this study is to investigate the impact of heatwaves on sea breeze, urban heat island intensity, and outdoor thermo-hygrometric comfort analysing ground-based remote sensing and in-situ meteorological measurements collected in a Mediterranean coastal metropolitan area (Rome, Italy) during the summer of 2022. The dataset (01 May - 31 August 2022) has been divided into heatwaves and not-heatwaves days to highlight the distinctive features of extreme heat episodes. Furthermore, the year 2022 was compared to 2020, the latter having been characterised by temperatures in line with the last two-decades.

The heatwaves do not significantly affect the onset time and the duration of sea breeze, while its cooling effect intensifies during the heatwaves. The urban heat island intensity (UHII) is evaluated by computing the hourly-averaged air temperature difference between two stations, one in the urban centre and the other in rural surroundings. Although the daily-averaged UHII does not show significant differences among the years under investigation and the subsets, marked differences can be identified in the urban heat island daily cycle. In fact, during daytime the highest temperatures are detected in rural inland areas while, at night, the city experiences higher temperatures, especially during the heatwaves. Finally, the Mediterranean outdoor comfort index suggests that a heatwave seems to be a not sufficient condition for human thermo-hygrometric stress, even if stronger discomfort is experienced during heatwaves.

1. Introduction

According to the World Meteorological Organization (WMO), a heatwave should be defined as “statistically unusual hot weather persisting for a number of days and nights” (WMO, 2022). Nevertheless, as this definition cannot be considered univocal and globally valid, several alternatives are found in the literature (see the review by Perkins, 2015) mainly based on: (i) intensity, i.e., the maximum air temperature reached during a heatwave event, (ii) temporal extension, i.e., the number of consecutive days that meet the chosen definition of heatwave, and (iii) frequency, i.e., the occurrence of excessive warming episodes per year or season. In addition, it is essential to consider also the geographical and climatic characteristics of the region under investigation. Although heatwaves are exceptional events, recent studies strongly suggested that, in the near future, these phenomena will become more frequent, intense, and prolonged (Lorenzo et al., 2021; Pörtner et al., 2022). The impact of long-lasting episodes of extreme heat is particularly evident

* Corresponding author.
E-mail address: annalisa.dibernardino@uniroma1.it (A. Di Bernardino).

https://doi.org/10.1016/j.uclim.2023.101735
Received 2 February 2023; Received in revised form 30 May 2023; Accepted 22 October 2023
Available online 2 November 2023

during summertime and in highly urbanised areas, where about 55% of the global population lives (UN, 2018), increasing hospitalisations and morbidity (Xu et al., 2016), requiring higher energy consumption for a massive use of Heating, Ventilation and Air-Conditioning (HVAC) systems (Ortiz et al., 2018a), reducing agricultural productivity (Lhotka et al., 2018), worsening air quality (Ordóñez et al., 2010) and thermal comfort (Zhou et al., 2020).

In large cities, these issues are further exacerbated because of the overlap with the Urban Heat Island (UHI) phenomenon, i.e., the increase in temperatures in built-up areas compared to the rural surroundings (Oke, 1982). The UHI is triggered by the coexistence of various factors, such as anthropogenic heat production, use of materials such as asphalt and concrete that absorb and retain heat, presence of buildings and obstacles that modify the ventilation and the atmospheric circulation close to the ground, low sky view factor with impact on solar radiation and longwave radiation absorption, and limited presence of green areas with reduction of evapotranspiration. The UHI can reduce the liveability of urban and suburban areas, contributing to human discomfort, health threats, and higher energy consumption, especially during summertime.

To characterize the UHI, the UHI intensity (namely UHII), i.e., the difference between the 2 m air temperature (typically hourly or daily averages) measured in the city and in one or more rural reference stations, is typically computed. Nevertheless, the choice of the stations is not straightforward as the site location, in terms of orography, land use, and thermal capacity, among others, can noticeably affect the results (Zhou et al., 2013; Cecilia et al., 2023). Although the UHI is widely studied, the interaction with the heatwaves is an important research question frequently debated in the literature and still open (Ward et al., 2016), with contradictory scientific outcomes. Several studies have shown that the UHII is not affected by the heatwaves (Zhao et al., 2014; Chew et al., 2021) since, during extreme hot events, despite the higher temperature experienced, no significant change in wind speed, soil moisture, and heat storage flux are found, especially in tropical cities (Chew et al., 2021). Otherwise, Oliveira et al. (2021) and Richard et al. (2021) showed a reduction in the UHII in conjunction with episodes of extreme warming. In contrast, Ortiz et al. (2018b), Jiang et al. (2019), and He et al. (2020) demonstrated the exacerbation of UHII during heatwaves because of the presence of persistent anticyclonic systems (Heaviside et al., 2015), low wind speed conditions (Li and Bou-Zeid, 2013), different heat convection efficiency in urban and rural environments (Zhao et al., 2014), and atmospheric stability (Tomlinson et al., 2012).

When coastal urban areas are investigated, the presence of the sea/land breeze regime must also be considered. The sea breeze develops when the difference in temperature between sea and land causes an onshore pressure gradient, determining the advection of cool and humid air masses from the sea to the warmer land (Simpson, 1994). The decrease in temperature due to the onset of the sea breeze can favour cooling, even during severe heatwaves (Papanastasiou et al., 2010), and can reduce thermal stress, contributing to the improvement of the pedestrian thermo-hygrometric wellbeing (Gershunov and Guirguis, 2012). Moreover, considering a coastal region, dry soil due to lack of rainfalls during heatwaves can enhance the sea/land thermal contrast, strengthening the sea breeze regime and fostering the advection of humid cold marine air (Stéfanon et al., 2014). Also, several studies have identified the soil-moisture deficit as one of the main drivers for the occurrence of extreme heat events, as it can affect the surface-energy balance (Fischer et al., 2007; Hirschi et al., 2011).

Although the above-mentioned topics have been extensively investigated in recent years, previous studies typically disjointedly explored the synergy between heatwaves and outdoor thermal comfort or sea breeze or UHI, usually focusing on social impacts and health (Vanderplanken et al., 2021; Hertig, 2020), on the effect of present and future climate change (Ialongo et al., 2008), and on the synoptic conditions driving severe heat episodes (Geirinhas et al., 2018; Satyanarayana and Rao, 2020; Xu et al., 2021; Pérez and García, 2023).

It is clear that the physical processes driving the interaction between all these fundamental aspects of the urban liveability are not yet fully understood and require further investigation, especially in the context of climate change. In light of this, this paper tries to fill these knowledge gaps by assessing the discomfort conditions caused by persistent abnormal high temperatures in a Mediterranean coastal metropolis, namely Rome (Italy). To the best of our knowledge, a comprehensive evaluation of the possible interactions between the main aspects of life in an urban environment is a novelty, especially for the Mediterranean Basin and for Italy.

The study, focused on the period 1 May − 31 August 2022, investigates in detail the differences between heatwave (hereinafter, HW) and not-heatwave (hereinafter, no-HW) days in terms of sea breeze development, UHII, and thermo-hygrometric wellbeing. To highlight the peculiar meteorological conditions of 2022, a similar analysis was also carried out for the period 1 May −31 August 2020, the latter having been characterised by temperatures in line with the reference period 2000–2019.

The manuscript is structured as follows: Sect. 2 describes the investigated area and the meteorological datasets, Sect. 3 depicts the method used for the identification of the heatwaves, the development of the sea breeze, the UHII, and the bioclimatic index considered for the assessment of thermo-hygrometric comfort. In Sect. 4, the results of the study are presented and discussed. Finally, the main conclusions of this paper are drawn in Sect. 5.

2. Material and methods

To identify the heatwave episodes and to evaluate their impact on sea breeze, UHII, and outdoor thermo-hygrometric comfort, the meteorological data provided by different stations located in the urban centre of Rome and in its surroundings are analysed.

2.1. Study area

The Mediterranean Basin is characterised by exceptional biodiversity and is recognised as a hotspot for climate change (Lionello and Scarascia, 2018). Its vulnerability to climatic hazards, mainly due to the geographical position in a transition zone between the temperate and rainy climate of central Europe and the arid climate of North Africa, concerns coastal climate-related risks, droughts,

and increase in surface temperatures (Lorenzo et al., 2021). Furthermore, projections show that rising temperatures will cause extreme weather events, such as heatwaves, which will be increasingly frequent, intense, and lasting (Lorenzo et al., 2021).

Being in the middle of the Mediterranean Sea (Fig. 1), Italy represents a geographical and climatological *unicum*, due to its complex orography and to the presence of mountain chains of the Apennines and the Alps, which operate as pathways and barriers for weather fronts and interact with synoptic winds (Fratianni and Acquaotta, 2017).

Rome (Lat. 41.91 N, Lon. 12.48 E), the capital of Italy, is located along the western coast of the Italian peninsula. The Rome city centre, about 27 km from the coast of the Tyrrhenian Sea, covers an area of about 1300 km^2 and is mainly flat, with an altitude between 13 and 140 m above sea level, while the rural areas surrounding the city have a more complex hilly orography. Due to its geographical position and its topography, the climate of Rome can be considered as temperate (Köppen-Geiger climate classification: Csa), characterised by dry and hot summers (Beck et al., 2018). The atmospheric circulation is governed by the sea breeze regime from the southwest, particularly evident during summertime under anticyclonic conditions, and by the drainage effect from the bottom of the Tiber valley responsible for northern winds (Petenko et al., 2011; Di Bernardino et al., 2021).

2.2. Meteorological datasets

The meteorological data of Rome are provided by the instruments hosted by the Boundary-layer Air Quality-analysis Using Network of Instruments (BAQUNIN) atmospheric supersite and installed on the rooftop of the Physics Department of "Sapienza" University of Rome (hereinafter named as SAP). More details about sensors, retrieval procedures, uncertainties, and quality assessment

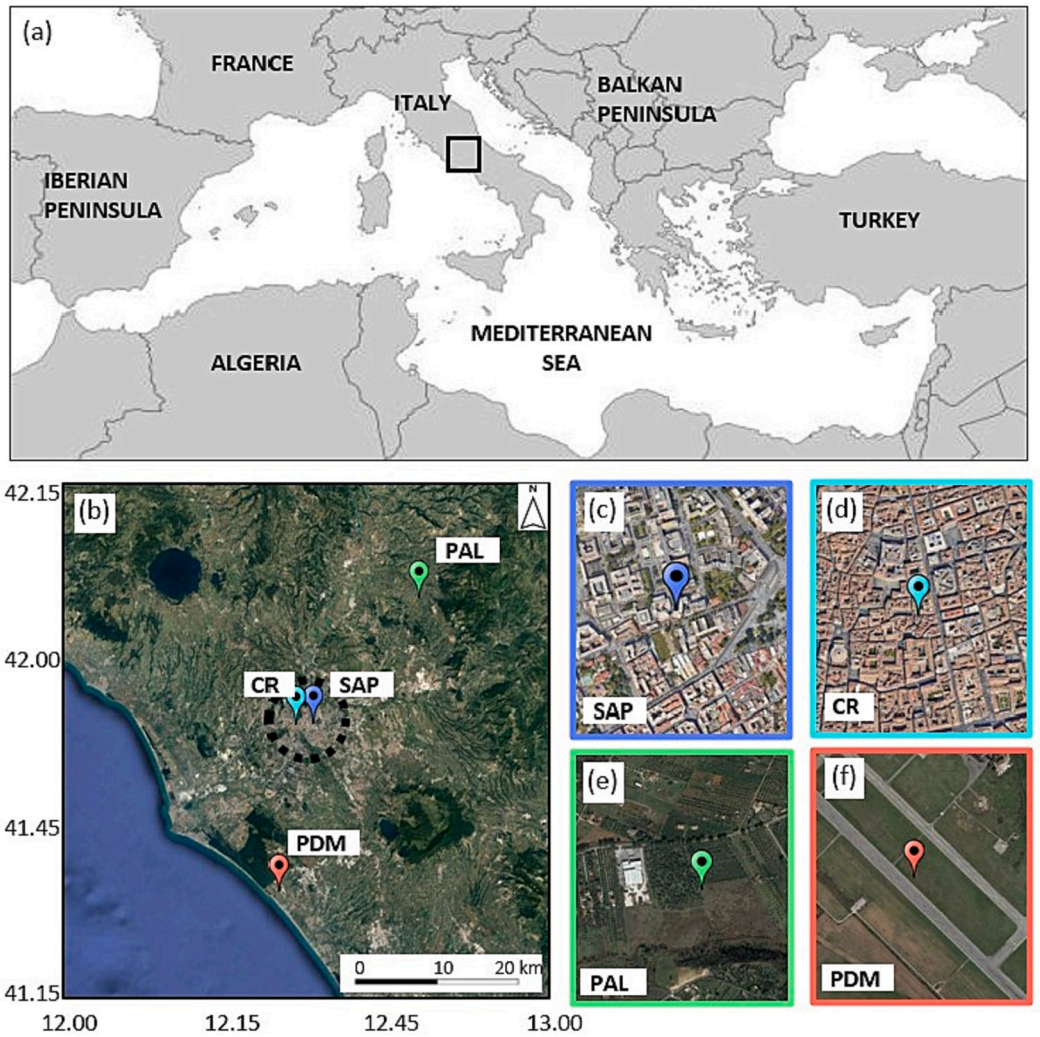

Fig. 1. (a) Geographic map of the Mediterranean Basin, the black square denotes the region under investigation. (b) Enlargement of the studied area and aerial photographs of the areas surrounding the urban (Physics Department of "Sapienza" University of Rome, SAP (panel c), Collegio Romano, CR (panel d)) and rural ((Palombara, PAL (panel e); Pratica di Mare, PDM (panel f)) meteorological stations. The black dotted circle in the panel b depicts the urban centre of Rome.

procedures can be found in Iannarelli et al. (2022) and in BAQUNIN (2023).

The detection of the heatwave events occurred during the summer months of 2020 and 2022 is carried out by analysing the 10-min-averaged surface observations of air temperature, relative humidity, wind speed, and wind direction collected by a ground-based weather station (Vaisala Weather Transmitter WXT520, Vantaa, Finland) belonging to the national private network Climate Network, managed by the OMD Foundation (Fondazione Osservatorio Milano Duomo, 2022), and hosted by SAP. SAP is located in a highly built-up area in downtown Rome and the station is WMO compliant, therefore the weather measurements can be used for the evaluation of heatwaves.

The development of the sea breeze front is evaluated by examining the vertical profiles of wind intensity and direction measured by the Doppler SOund Detection And Ranging (SODAR). All profiles have a vertical resolution of 18.5 m and are averaged over 10-min intervals.

The pyranometer (SR11, Hukseflux Thermal Sensor company, Delft, the Netherlands) measures the global solar radiation in the 285–3000 nm spectral range, required for the calculation of the thermo-hygrometric comfort index, with 5-s resolution. The pyranometer is calibrated at Physical Meteorological Observatory in Davos (PMOD) World Radiation Center (WRC) on bi-annual basis, showing excellent radiometric stability.

To evaluate the UHII, the temperature time series of the Palombara weather station (hereinafter PAL), belonging to the Integrated Agrometeorological Service of the Lazio Region (ARSIAL, 2022) micrometeorological network, are used in addition to those of SAP. The PAL station is equipped with CR1000 Campbell sensors (Campbell Scientific Europe, Loughborough, U.K.), following the WMO guidelines. The hourly-averaged measurements of air temperature are quality-checked and provided by ARSIAL.

To assess the extension and spatial homogeneity of the heatwaves and to identify any effects of orography and distance from the coastline, the hourly-averaged time series of air temperature measured at the Italian Air Force station of Pratica di Mare (hereinafter PDM, ICAO CODE: LIRE) are analysed. The station, WMO compliant, is about 26 km south of Rome and 2 km inland from the coast. Data are quality-checked and provided by the meteorological service of the Italian Air Force.

Finally, the identification of the heatwaves is based on the computation of temperature anomalies with respect to a long time series, used as a reference. Here, the reference dataset is the time series collected at the Collegio Romano (hereinafter CR) station, hosted by the Historical Meteorological Observatory in downtown Rome. The weather station, operated under the responsibility of CREA (Consiglio per la Ricerca in Agricoltura e l'Analisi dell'Economia Agraria, 2022), provided the hourly-averaged temperatures for the period 2000–2019. This dataset has already been used in Di Bernardino et al. (2022a) to identify meteorological temporal trends in Rome and has, therefore, already been subjected to quality check processes and data homogenization. The CR station is about 2.5 km from SAP and, being both installed on buildings' roofs in highly built-up areas, they can be considered as representative of the same environmental conditions. Details about the data pre-processing and the homogenization procedure can be found in Di Bernardino et al. (2022a).

The temporal resolution of all the meteorological data was uniformed, resulting in hourly and daily datasets. Table 1 summarizes the main information about the stations and datasets used in this study.

Table 1
List of the stations considered in the present study and measured variables.

Station	Lat. N	Lon. E	Altitude (m a.s.l.)	Environment	Variables	Period
Sapienza (SAP)	41.90	12.51	75	urban	Surface: air temperature, relative humidity, wind speed, wind direction. Global solar radiation Vertical profiles: wind speed and wind direction.	01/05/2020–31/08/2020 01/05/2022–31/08/2022
Palombara (PAL)	42.07	12.74	142	rural	Surface air temperature	01/05/2020–31/08/2020 01/05/2022–31/08/2022
Pratica di Mare (PDM)	41.65	12.44	12	coastal	Surface air temperature	01/05/2020–31/08/2020 01/05/2022–31/08/2022
Collegio Romano (CR)	41.90	12.48	57	urban	Surface air temperature	01/01/2000–31/12/2019

3. Data processing

3.1. Identification of heatwaves

As mentioned in the Introduction, a comprehensive heatwave definition valid worldwide has not yet been established. Here, different approaches for the detection of the heatwaves are applied by identifying the values that exceed the 95th percentiles of the average (T_{ave}), maximum (T_{max}), and minimum (T_{min}) daily temperatures during the summer periods of 2020 and 2022, compared to the twenty-year reference dataset.

Therefore, an intense heat event is classified as a heatwave if it meets the two criteria detailed below:

(i) Temperature constrain:

$$T_i > \left(\widetilde{T}_{i,ref}\right)_{95} \quad (1)$$

where T_i is the daily (average, T_{ave}, maximum, T_{max}, or minimum, T_{min}) temperature of the i-th day of the year and $\left(\widetilde{T}_{i,ref}\right)_{95}$ is the 95th percentile of the probability density function related to the long-term period, chosen as a reference (i.e., 2000–2019 at the CR urban station). The probability distribution function is found by computing, for each day of the year, the daily average, minimum, and maximum temperatures as a moving average over a time window of 20 days, centred on the day under investigation, and then the 95th percentile is calculated.

(ii) Temporal constrain: exceeding the temperature constrain must occur for at least 4 consecutive days.

This definition, based on Stéfanon et al. (2012), meets the temporal limit proposed by the WMO and is more stringent than other proposals found in the literature. As discussed in the following sections, T_{ave} is chosen as the most representative thermal variable for extreme heat events, as it allows to include both the extreme heat episodes identified only by the analysis of T_{min} and T_{max}. Preliminary tests have been carried out varying the time window used for the moving average between 4 and 30 days. The final time window is set at 20 days, to capture both the short-term variations characteristic of extreme heat events and the long-term variability of the synoptic dynamics, according to Stéfanon et al. (2012).

The characteristics of each heatwave have been quantified following the indices proposed by Fischer and Schär (2010), here adapted to the analysis of a single summer, i.e.:

- heatwave duration (HWD): number of consecutive days meeting the heatwave criteria;
- heatwave amplitude (HWA): maximum daily-averaged temperature anomaly compared to the reference period;
- heatwave average amplitude (HWAA): average temperature anomaly compared to the reference period;
- hot days (HD): number of days with maximum temperature exceeding 35 °C;
- tropical nights (TN): number of days with minimum temperature exceeding 20 °C;
- combined hot days and tropical nights (CHT): number of days with concurrent HD and TN.

Finally, as mentioned in the Introduction, to highlight the peculiarities of extreme heat events, each summer dataset has been divided into two subsets. The former gathers all the days identified as heatwave (namely, HW), while all the remaining days of the investigated period belong to the latter subset (namely, no-HW).

3.2. Development of the sea breeze

The area under investigation is mainly flat and the Tyrrhenian coast, about 30 km from downtown Rome, has a northwest-southeast orientation (see Fig. 1). According to Di Bernardino et al. (2021) and Petenko et al. (2011), the centre of Rome is grasped by the sea breeze front and, therefore, it can reasonably be assumed that the observations collected at SAP are affected by the sea breeze regime.

The development of the sea breeze front over the city is based on the analysis of the vertical profiles of wind intensity and direction measured by the SODAR and of the thermo-hygrometric parameters collected by the weather station at SAP, following the criteria listed and discussed in Di Bernardino et al. (2021). According to Di Bernardino et al. (2021), a day is classified as “sea-breeze day” if a significant increase in wind speed and a change in wind direction, which must blow perpendicularly to the coastline, are observed in conjunction with a reduction in temperature and an increase in specific humidity. These variations typically occur between 08:00 UT and 12:00 UT, i.e., in the period typically involved by the onset of the breeze front (Di Bernardino et al., 2022b), and last until the afternoon (16:00 UTC - 20:00 UTC), i.e., when the sea breeze regime ceases because of the reduction of solar radiation and, therefore, of thermal convection. All days with rain lasting at least 10 min (identified by the visual inspection of the SODAR signal plots) are excluded from the following analysis. However, rainy days represent only 2.4% and 4.1% of the total summer days during 2020 and 2022, respectively, without a statistically significant impact on the results.

3.3. Urban Heat Island Intensity

The Urban Heat Island Intensity (UHII) is obtained following the traditional definition (Stewart, 2011), i.e., by computing the difference between the hourly-averaged air temperatures measured at two fixed in-situ stations, one in the urban centre (T_{urb}) and the other in rural surroundings (T_{rur}), as defined in Eq. (2):

$$UHII = T_{urb} - T_{rur} \quad (2)$$

In this context, the choice of the stations is not straightforward, and the selection is performed by rearranging the constrains proposed by Possega et al. (2022) for the investigation of the synergy between heatwaves and UHII in several European cities:

- the distance of the stations from the city centre must be less than 10 km for the urban station and 35 km for the rural station;
- the altitude difference between the selected urban and rural stations, necessary to remove the impact of topography on UHI evaluation, must be less than 70 m;
- the rural station must be surrounded by natural, not densely built-up areas.

The SAP and PAL stations meet the above-mentioned criteria, allowing for the correct evaluation of the UHII. The altitude difference between SAP and PAL is 67 m, i.e., it is considerable although below the threshold proposed by Possega et al. (2022). Nonetheless, these stations can be assumed as suitable for this study as the focus is on the summer periods, characterised by persistent high-pressure systems, so without requiring corrections in the calculation of the night-time UHII (Martin-Vide et al., 2015). Results refer both to the time series of daily-averaged UHII and to the average daily cycle of the UHII.

3.4. Mediterranean outdoor comfort index

According to ASHRAE (ASHRAE Standard 55, 2013), the outdoor thermal comfort is the "condition of mind that expresses satisfaction with the thermal environment and is assessed by subjective evaluation". The level of thermal comfort experienced by the population during the heatwaves can be assessed with a series of bioclimatic indices, based on the combination of physiological and environmental factors. Among such indices, the Mediterranean Outdoor Comfort Index (MOCI) is established for the Mediterranean normo-type (Salata et al., 2016) and is defined as in Eq. (3):

$$MOCI = -4.257 + 0.146 \bullet T_A + 0.325 \bullet I_{CL} + 0.005 \bullet RH + 0.001 \bullet I_S - 0.235 \bullet W_S \quad (3)$$

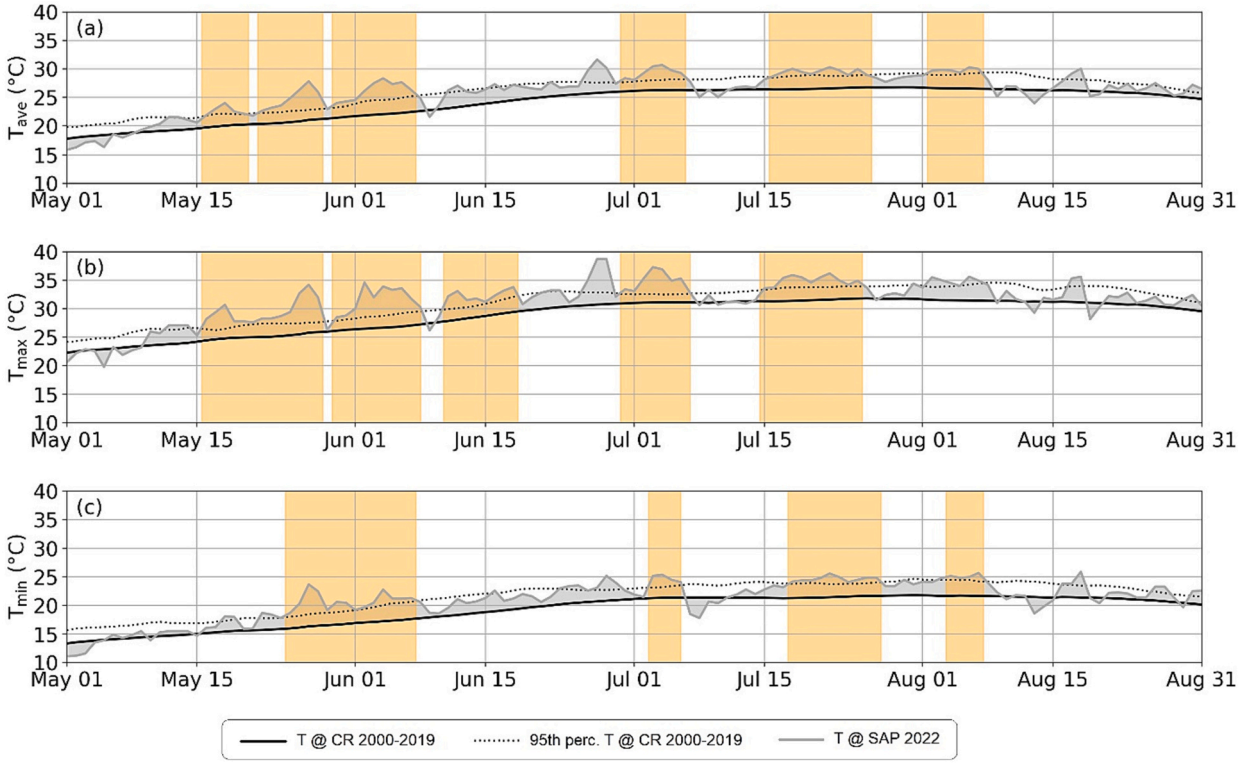

Fig. 2. Time series of daily average (T_{ave}, panel a), maximum (T_{max}, panel b), and minimum (T_{min}, panel c) air temperatures measured in the reference period 2000–2019 at the CR station (black line) and at SAP during summer 2022 (grey line). The dotted line shows the 95th percentile of the probability distribution function of the reference dataset, the grey shaded areas highlight the temperature anomalies with respect to the reference period, and the orange vertical bands depict the events of heatwave.

with:

$$I_{CL} = 1.608–0.038 \bullet T_A \quad (4)$$

where T_A is the 2 m air temperature (°C), I_{CL} is the thermal resistance of the clothing (°C), RH is the 2 m relative humidity (%), I_S is the global solar irradiance (W/m^2), W_S is the 10 m wind speed intensity (m/s).

The MOCI is experimentally defined and is based on an ASHRAE 7-point scale, with values in the $-0.5 \div 0.5$ range corresponding to different thermal comfort conditions. MOCI values lower than −0.5 or higher than 0.5 implies cold or hot discomfort, respectively. A detailed description of this index and its development can be found in Salata et al. (2016).

The hourly-averaged MOCI values, calculated according to Eq. (3) using the measurements collected from the SAP weather station for 2022 and 2020, are used to compute the MOCI daily maximum, being the latter assumed as representative of the worst daily thermo-hygrometric conditions.

4. Results and discussion

4.1. Description of meteorological conditions during summer 2022 and 2020

During the summer months of 2022 particularly high temperatures, scarce precipitations, and low cloud coverage were experienced over the Italian peninsula (CNR-ISAC, 2023). From the first ten days of May to the end of July, a persistent continental subtropical high-pressure system expanded towards the central Mediterranean and Italy. In this period, the 500 hPa geopotential height maps clearly showed a very pronounced increase in height of the North African high-pressure system, due to intense advection of warm air masses from Africa. This resulted in high surface temperatures and poor rainfalls. Otherwise, in August, the transit of north-Atlantic troughs and the expansion of the Azores anticyclone allowed for the advection of fresh and unstable air, responsible for the thermal drop towards the climatological averages of the period (COPERNICUS, 2022). As an example, Fig. S1 shows the 500 hPa geopotential height maps referred to 19 June and 22 August 2022, chosen as days representative of the two peculiar meteorological phases.

As shown in Fig. 2, during 2022, T_{ave}, T_{max}, and T_{min} remained well above the 95th percentile for several consecutive days. In particular, T_{ave}, selected as the reference variable for identifying heatwaves as discussed in Sect. 4.2, exceeded T_{ref} in 86.2% of the 2022 summer days under investigation.

The exceptional warm conditions of the 2022 summer period are also noticeable by the values in Table 2: during May, the absolute maximum hourly temperature exceeded the value of the 2000–2019 period by 7.9 °C. In terms of maximum temperatures, the discrepancy with respect to the reference twenty-year period decreased as the summer progressed (+4.0 °C in August). The 95th percentile also confirmed the exceptional heat experienced in May (+4.8 °C) and June (+4.0 °C), corroborating the unusual long spells of exceptionally high temperatures in the early summer. The average monthly temperatures follow a similar trend: the maximum deviation with respect to the reference period was recorded in June (+2.9 °C), while the minimum was in August (+1.2 °C). Furthermore, the year 2022 was characterised by an intense temporal variability and a high temperature excursion. Also, the minimum hourly temperatures were always lower than the reference dataset, except for June (+1.7 °C). This latter aspect is attributable to short-term low-pressure systems that characterised the cooler summer days, as can also be observed from the time series in Fig. 2c.

On the other hand, during summer 2020 the situation was considerably different. From the atmospheric dynamics, the period from 01 May to 31 August 2020 was characterised by two distinct meteorological phases: the former, very unstable and cool during May,

Table 2
Descriptive statistics of daily temperatures measured at SAP (summer 2020 and 2022) and at CR (2000–2019). All the values are expressed in °C. The indicators exceeding, equal, and below the reference values are shown in red, blue, and green, respectively.

	MAY			JUNE			JULY			AUGUST		
	2000-2019	2020	2022	2000-2019	2020	2022	2000-2019	2020	2022	2000-2019	2020	2022
Average	19.7	19.7	21.4	24.0	24.0	26.9	26.5	26.5	28.5	26.1	26.1	27.3
Standard deviation	2.6	1.1	3.1	1.4	1.4	1.9	0.2	0.2	1.5	0.5	0.5	1.8
Minimum	13.3	13.3	11.1	16.9	16.9	18.6	21.1	21.1	17.8	20.2	20.2	18.6
Maximum	26.3	26.3	34.2	30.9	30.9	38.7	31.8	26.8	37.3	31.6	31.7	35.6
50th percentile	19.8	19.8	21.8	24.0	24.1	26.9	26.4	26.4	28.8	26.3	26.3	27.0
95th percentile	21.4	21.4	26.2	26.0	26.0	30.0	26.8	26.8	30.4	26.6	26.7	30.0

June, and the first half of July; the latter, much hotter and without significant low-pressure systems from the end of July to the end of August. In Fig. S2, the 500 hPa geopotential height maps referred to 30 May and 17 August 2020, chosen as examples of the two meteorological phases, are shown. The air temperatures fluctuated around the long-term average in the first half of June and in the central period of July, when many days with average, maximum, and minimum temperatures below the long-period reference values occurred. The 95th percentile was exceeded only for short periods in mid-May, late July, and August (Fig. 3). In all the considered cases, the exceedances were limited in time and interspersed with cool periods. Contrariwise, in August rainfall was scarce and temperatures were often above the twenty-year averages. The values shown in Table 2 highlight the likeness between the thermal conditions of 2020 and the reference period: the average, minimum, and maximum monthly temperatures are perfectly in line with the long-term values, except for T_{max}, which in July records −5.0 °C and in August +0.1 °C. The monthly 50th and 95th percentiles are also comparable with the reference period and only in August the 95th percentile shows an increase of 0.1 °C in 2020.

The time series in Fig. 3 and the values in Table 2 point out that summer 2020 was characterised by thermal conditions perfectly comparable and overlapping with the twenty-years reference period and, consequently, it can be selected as a comparison year to highlight the effects due to the exceptional heat of 2022.

4.2. Detection of the heatwaves

As shown by the orange bands in Fig. 2 and as summarised in Table 3, assuming T_{ave} as the most representative thermal variable, during 2022 six heatwaves are detected, covering 26.6% of the period examined. Heatwaves are found during each month, even if they are more frequent in the second half of May and in the first ten days of June when, except for three days (15, 21, and 29 May), the definition of heatwave is always met. The duration of the events ranges between 5 (HW#1) and 11 days (HW#5), whereas for HW#2 the most intense anomalies compared to the reference dataset (HWA = 5.0 °C and HWAA = 2.3 °C) are observed. All the events between the second half of May and the first ten days of June, i.e., 50% of the total, do not record HD, suggesting that the temperatures have been exceptionally high compared to the twenty-year period but not so high as to fall within the definition of HD. Conversely, only for HW#1 TN were not detected. Moving towards the summer peak, the heatwaves are characterised by lower temperature anomalies, but all have at least 50% of HD and 100% of TP.

During summer 2020, four severe warm episodes are classified as heatwaves between the end of July and August, i.e., in the typically hottest period for the studied area. Each heatwave lasts at most 5 days, i.e., just above the temporal threshold used for the detection. HWA and HWAA are lower than during 2022 (HWA and HWAA maximum values equal to 2.5 °C and 1.3 °C, respectively, during HW#4). Apart from HW#1, characterised by 80% of hot days, HDs are always below 25%. On the contrary, 100% of tropical

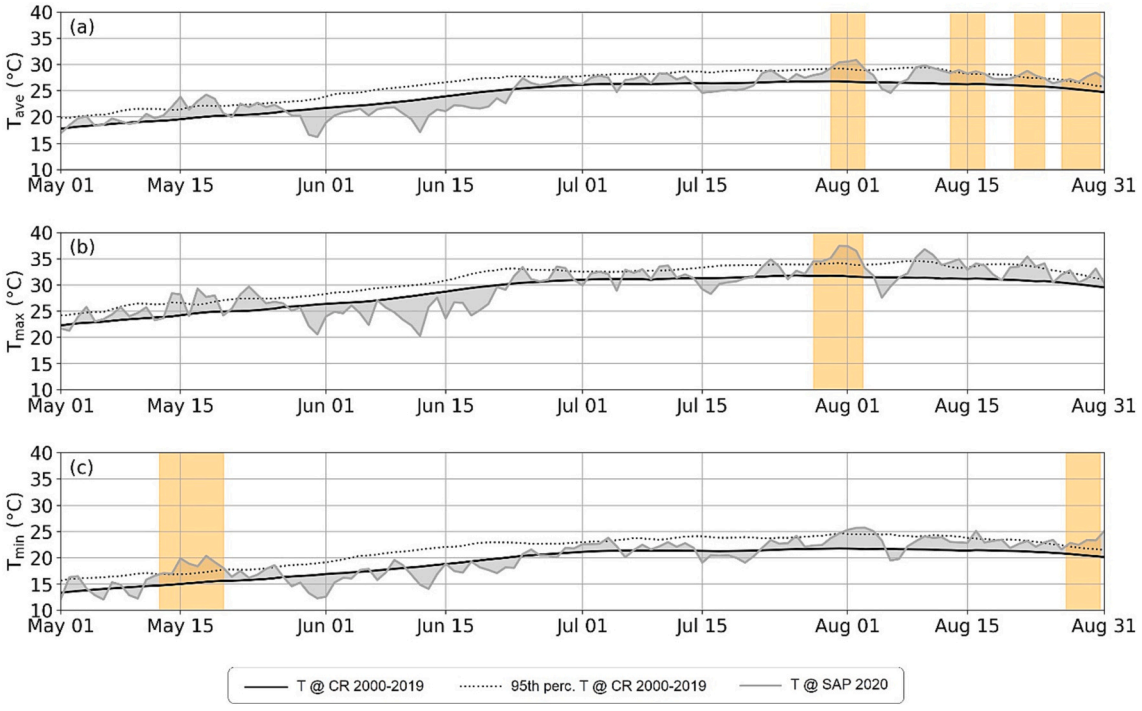

Fig. 3. Time series of daily average (T_{ave}, panel a), maximum (T_{max}, panel b), and minimum (T_{min}, panel c) air temperatures measured in the reference period 2000–2019 at the CR station (black line) and at SAP during summer 2020 (grey line). The dotted line shows the 95th percentile of the probability distribution function of the reference dataset, the grey shaded areas highlight the temperature anomalies with respect to the reference period, and the orange vertical bands depict the events of heatwave.

Table 3
Descriptive indices for the heatwaves identified in the summer 2022 and 2020 using T_{ave} as indicator. The date of start and stop of each event, together with the heatwave duration (HWD), heatwave amplitude (HWA), heatwave average amplitude (HWAA), hot days (HD), tropical nights (TN), and combined hot days and tropical nights (CHT) are given.

Year	Event ID	Start	Stop	HWD (n. days)	HWA (°C)	HWAA (°C)	HD (n. days)	TN (n. days)	CHT (n. days)
2022	HW#1	16/05	20/05	5	1.9	0.7	0	0	0
	HW#2	22/05	28/05	7	5.0	2.3	0	3	0
	HW#3	30/05	07/06	9	3.8	1.9	0	7	0
	HW#4	30/06	06/07	7	2.6	1.5	4	7	4
	HW#5	16/07	26/07	11	1.6	0.7	6	11	6
	HW#6	02/08	07/08	6	1.1	0.8	3	6	3
2020	HW#1	29/07	02/08	5	1.9	1.0	4	5	4
	HW#2	13/08	16/08	4	0.5	0.3	0	4	0
	HW#3	20/08	23/08	4	1.3	0.5	1	4	1
	HW#4	26/08	30/08	5	2.5	1.3	0	4	0

nights are recorded during three out of four heatwaves, underlining the nocturnal discomfort conditions of the urban area due to the UHI effect. The CHT values suggest that HW#1 was the worst heatwave from the point of view of the thermal load since, although it assumed low HWA and HWAA values (1.9 °C and 1.0 °C respectively), it recorded day and night temperatures above the discomfort thresholds.

4.3. Assessment of discomfort during heatwaves

4.3.1. Sea breeze

The SODAR vertical wind speed and direction profiles and the in-situ thermo-hygrometric variables reveal that, during 2022, the urban area of Rome was grasped by the sea breeze in 73.2% of days under investigation. In this period, the atmospheric circulation was governed by the sea breeze regime on 84.5% of the cases, followed by southern synoptic winds (11.1%). The remaining 4.4% of cases were characterised by variable wind direction throughout the day. As an example, Fig. S3 shows the temporal variation of meteorological parameters for HW#4 of summer 2022. Specifically, the 10-min averaged wind velocity and direction as measured by the SODAR at 36.2 m above ground level (panel a), the surface average temperature (panel b), and the specific humidity (panel c) are given.

The same analysis, conducted for the summer months of 2020, shows that the sea breeze reached downtown Rome on 63.6% of the days investigated. During the heatwave episodes, the atmospheric circulation allowed for the development of the sea breeze in 66.7% of the days, while in the remaining 33.3% of the cases the atmospheric dynamics was dominated by southerly winds.

In this Section, only days for which the SODAR and the meteorological station allowed for the detection of the sea breeze are considered. The analysis is carried out for the resulting dataset, in turn identifying the HW and no-HW sub-datasets. Firstly, the variations in wind intensity and direction at the first SODAR measurement altitude (36.2 m from the ground) are inspected to evaluate the average and median onset time, duration, and offset time of the sea breeze (see Table 4). To evaluate the cooling effect due to the development of the sea breeze (recalling that the time series of temperature and surface wind have hourly resolution), the time frame 11:00–19:00 UTC is chosen as representative for both years and for all the sub-datasets under investigation.

In 2022, for the selected temporal range, the surface wind average intensity was 2.2 m/s and reached a maximum intensity of 5.9 m/s, also in this case with no significant differences among HW and no-HW (Table 4). In 2020, the anemological results were similar: the average wind speed during the sea breeze was 2.6 m/s with a maximum of 6.2 m/s (Table 4). The differences between the sub datasets were quite small. These outcomes suggest that the heatwaves do not affect neither the sea breeze onset/offset time nor its intensity. Moreover, the air temperatures measured at SAP have been used to evaluate the cooling effect due to the development of the sea breeze. Over the period 11:00–19:00 UTC, the temperature decreased on average by 4.7 °C both in 2022 and 2020. The reduction was more intense during heatwaves (5.2 °C and 5.8 °C in 2022 and 2020, respectively) than during no-HW days (4.4 °C in 2022 and 2020).

Table S1 shows the same analyses conducted for each individual heatwave identified in 2022 and 2020. The heatwaves are often

Table 4
Statistics for sea breeze for all sea-breeze days, HWs, and no-HW days during 2022 and 2020.

Year	Dataset	Start time UTC		Stop time UTC		ΔT (°C)	Wind speed (m/s)		
		Average	Median	Average	Median		Average	St. Dev.	Max.
2022	all sea breeze days	11:22	11:20	18:44	19:00	4.7	2.2	0.3	5.9
	HW days	11:26	11:20	18:44	18:55	5.2	2.2	0.3	6.0
	no-HW days	11:19	11:20	18:43	19:00	4.4	2.2	0.3	5.9
2020	all sea breeze days	11:25	11:20	19:01	18:55	4.7	2.6	0.4	6.2
	HW days	11:36	11:30	19:18	19:05	5.8	2.8	0.1	6.0
	no-HW days	11:22	11:10	18:57	18:50	4.4	2.5	0.4	6.3

characterised by sea breeze (occurrence greater than 50% in all cases, except for HW#4 of 2020) but without significant variations on the onset time, average and maximum wind intensity. On the contrary, the individual events show greater variability in the offset time (between 16:58 for HW#2 of 2022 and 20:06 for HW#1 of 2020) and in the cooling effect. The latter varies between 5.4 °C (HW#2) and 6.2 °C (HW#3) in 2020 and between 4.6 °C (HW#1) and 5.4 °C (HW#5) in 2022.

To confirm the regional extent of heatwaves, the time series of the air temperatures measured at the SAP (urban), PDM (coastal), and PAL (rural) stations for 2022 (Fig. 4a) and 2020 (Fig. 4b) are presented. The solid lines depict the average daily temperatures, while the shaded areas highlight the daily temperature range. SAP recurrently experienced the highest average temperatures due to the presence of urban fabrics and, therefore, of the UHI. The other stations assume similar patterns with comparable increase/decrease rates, even during most of the heatwaves.

4.3.2. Urban Heat Island Intensity

The UHII is evaluated by computing the air temperature difference between the urban (SAP) and rural (PAL) stations. To account for the effect of the sea breeze regime on UHII, only the days identified in the previous Section as sea breeze days are considered.

As shown in Fig. 5, the daily average temperatures are always higher in downtown Rome than in the rural surroundings (except for 16/05/2020), as expected in the case of a city subject to the UHI (Cecilia et al., 2023). During the period 01 May – 31 August 2022, the UHII ranges between 0.8 °C and 4.3 °C, assuming an average value of 2.2 °C, and seldom exceeding 3 °C. Differences among months are not detectable. During the summer period of 2020, apart from a day in which the rural area was warmer than the city centre, resulting in a negative UHII equal to −0.6 °C, the UHII ranges between 0.7 °C and 3.5 °C, with an average intensity of 1.8 °C. During the HW days, the UHII is on average equal to 1.5 °C, while in the case of no-HW it increases up to 2.0 °C.

To deepen the analysis of the relationship between UHI and heatwaves, Fig. 6 shows the daily cycle of average temperature at SAP and PAL, for the HW and no-HW sub datasets and the related daily cycles of UHII for 2022 and 2020.

Specifically, it can be noted that the air temperature is higher during HW than no-HW days both in urban and rural environments, as expected in the case of severe warm episodes. One of the most interesting aspects, however, is what happens during daytime: in Rome city centre, the arrival of the sea breeze front at 11:00 UTC favours cooling and, therefore, triggers the decrease in temperature from 11:00 UTC onwards. On the contrary, the rural inland area, not grasped by the sea breeze, continues to warm up in the morning until 13:00 UTC, i.e., when the maximum incoming solar radiation is reached. This implies that the rural area, despite being characterised by natural land use, without buildings and/or obstacles and, hence, without UHI, records daytime maximum temperatures

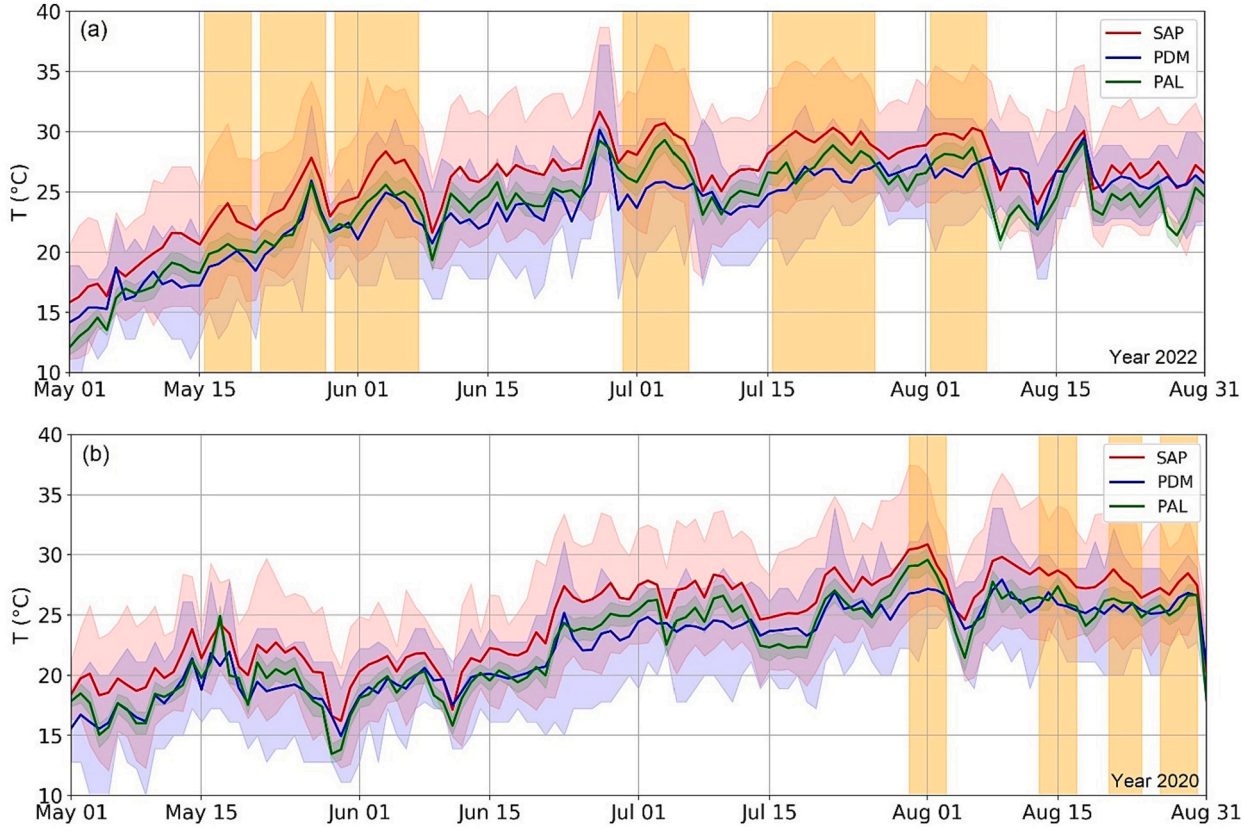

Fig. 4. Time series of daily-averaged air temperature (solid lines) and daily temperature range (shaded areas) measured at the urban (SAP), coastal (PDM), and rural (PAL) stations for 2022 (panel a) and 2020 (panel b). Orange vertical bands depict the heatwaves.

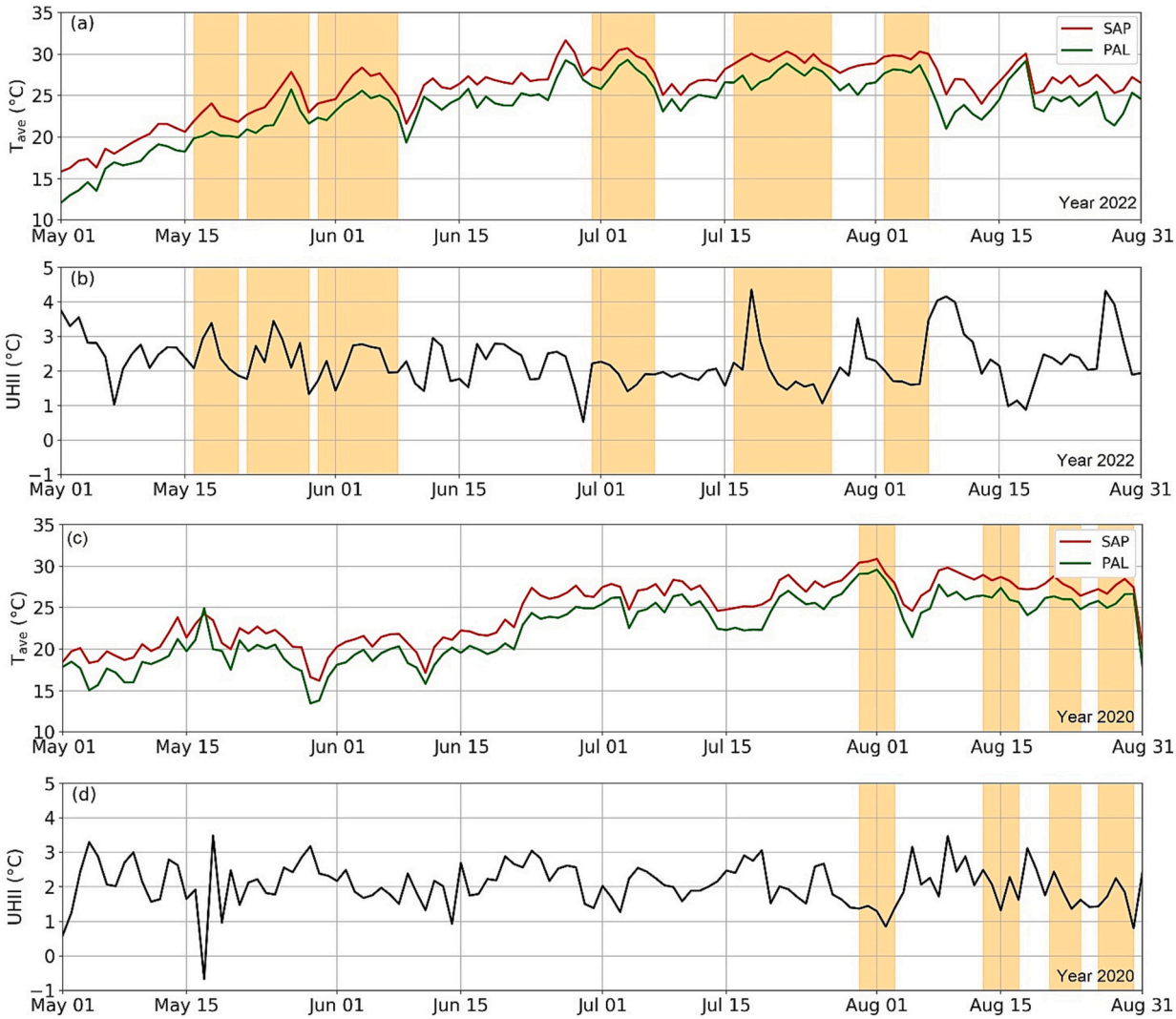

Fig. 5. Time series of daily-averaged air temperature measured at the urban (SAP) and rural (PAL) stations for 2022 (panel a) and 2020 (panel c) and UHII for 2022 (panel b) and 2020 (panel c). Orange vertical bands depict the heatwaves.

higher than the city centre. In contrast, during night-time, the city is warmer than the rural surroundings because of the UHI which, as it is known, limits the nocturnal cooling of the atmosphere close to the ground (Possega et al., 2022). The behaviour is similar in 2022 (Fig. 6a) and 2020 (Fig. 6c), although during 2022 urban and rural temperatures show more limited differences. This aspect might be attributable to the persistence of severe heat conditions, which have reduced the possibility of cooling for rural areas and would require further investigations. Observing the temporal evolution of the UHII, evident variances between diurnal and nocturnal behaviour are notable, which are totally lost by analysing only the daily-averaged values of UHII. Indeed, the UHII reaches a peak of about +6 °C before the sunrise and a minimum between −1.9 °C (no-HW in 2022) and − 3.9 °C (HW in 2020) at 14:00 UTC.

Comparing the trends of 2022 and 2020 it can be noted that, while in 2020 the UHI was more intense during the heatwaves throughout the day, in 2022 there is a reversal. In fact, during the night the UHII is higher in HW than in no-HW, further demonstrating the urban heating compared to the rural area, while during the day the temperature difference between SAP and PAL is lower. These results are very noteworthy as they allow us to highlight the contribution of the sea breeze and heatwaves on diurnal and nocturnal UHII.

4.3.3. Mediterranean outdoor comfort index

Fig. 7 shows the daily maximum values of MOCI for 2022 and 2020. From 10 June 2022 onwards, all days (except for 19 August) are in the discomfort range regardless of the heatwave's occurrence, with maximum MOCI during heatwaves. Before that date, some days falling within the heatwave definition do not present hot discomfort conditions.

During summer 2020, overheating situations occurred only from the end of June onwards, except for a few days at mid-July,

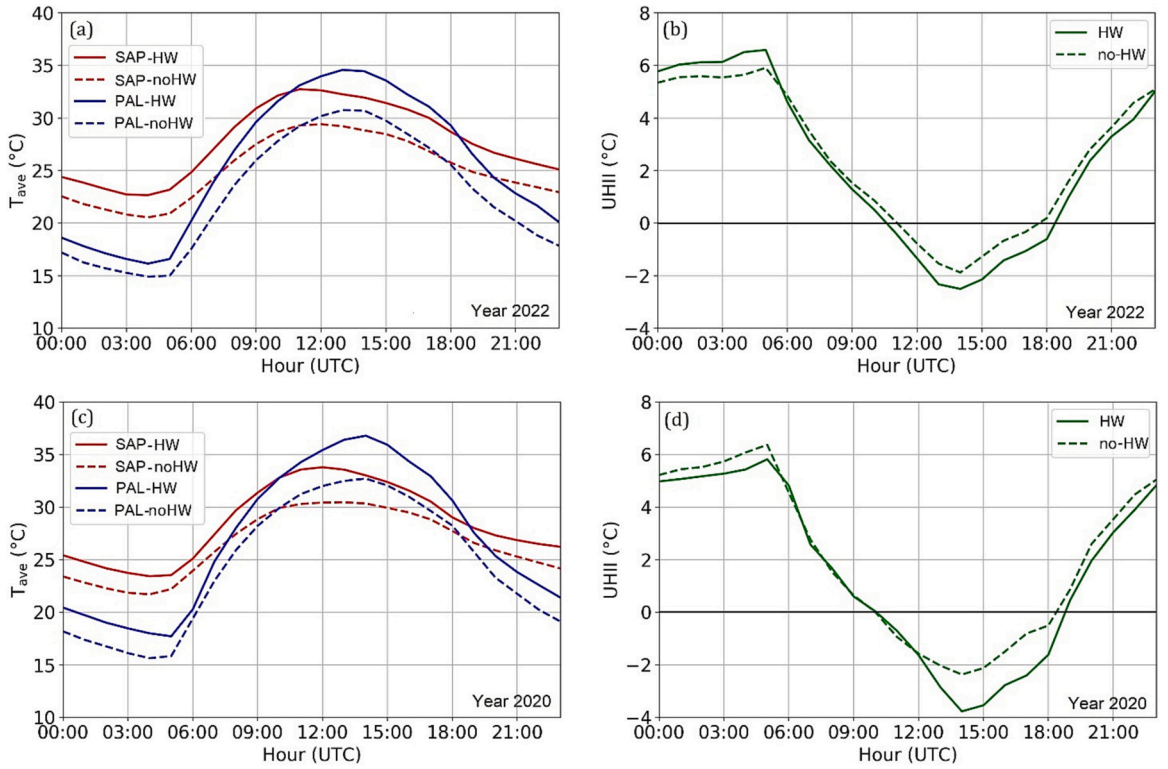

Fig. 6. Temporal evolution of hourly-averaged temperatures at SAP and PAL for HW and no-HW sub datasets in 2022 (panel a) and 2020 (panel c) and temporal evolution of UHII for HW and no-HW sub datasets in 2022 (panel b) and 2020 (panel d).

beginning, and end of August. The first part of the summer was characterised by good thermal conditions and between June and July there were even five days with MOCI<-0.5.

5. Discussion

This paper presents a synergic assessment of the heatwave events on sea breeze development, urban heat island intensity, and outdoor thermo-hygrometric comfort during the season May–August 2022 in Rome (Italy), providing a benchmark for understanding the interactions among the main aspects of urban liveability in the framework of climate change.

In the investigated area, the period analysed was characterised by the prolonged presence of high-pressure systems, scarce rainfalls, and low cloud coverage. According to the criteria assumed in this study and presented in Section 3.1, six heatwaves are identified during the summer period of 2022, with duration between 5 and 11 days and average temperature anomaly compared to the reference period up to 2.3 °C. In the same period of 2020, four heatwaves are recorded, with a maximum duration of five days and intensity well below the events of 2022. The findings reveal not only the extraordinary intensity and lasting of the heatwaves in 2022 but also the early onset of the summer season associated with high temperatures during May and June.

The implications and consequences of the progressive advance of the start of the summer season are manifold, involving numerous aspects of human life, and strongly suggest careful consideration.

5.1. Sea breeze regime

The analysis shows that the heatwaves, although being prolonged and very intense, do not significantly affect the onset, duration, and intensity of the sea breeze. On average, the sea breeze front reaches downtown Rome between 11:00 and 19:00 UTC, without significant differences among the two years investigated and with variations of less than 10 min among the HW and no-HW cases. The onset and offset times of the breeze identified in the present study agree perfectly with those found for the same region by Cecilia et al. (2023) using a dense in-situ weather station network. Furthermore, the estimated cooling amplification during heatwaves agrees with findings by Giannaros et al. (2023) in Athens (Greece) during summer 2021. Also, Papanastasiou et al. (2010) identified in Volos (Greece) a marked beneficial effect from the concomitance of heatwaves and sea breeze circulation, producing a maximum temperature decrease of 8.2 °C in the warmest hours of the day.

The data acquired at SAP, PDM, and PAL, i.e., in stations with different degree of urbanization and different distance from the coast, points out that the heatwaves are mainly related to synoptic-scale systems and, therefore, cause large-scale atmospheric warming that

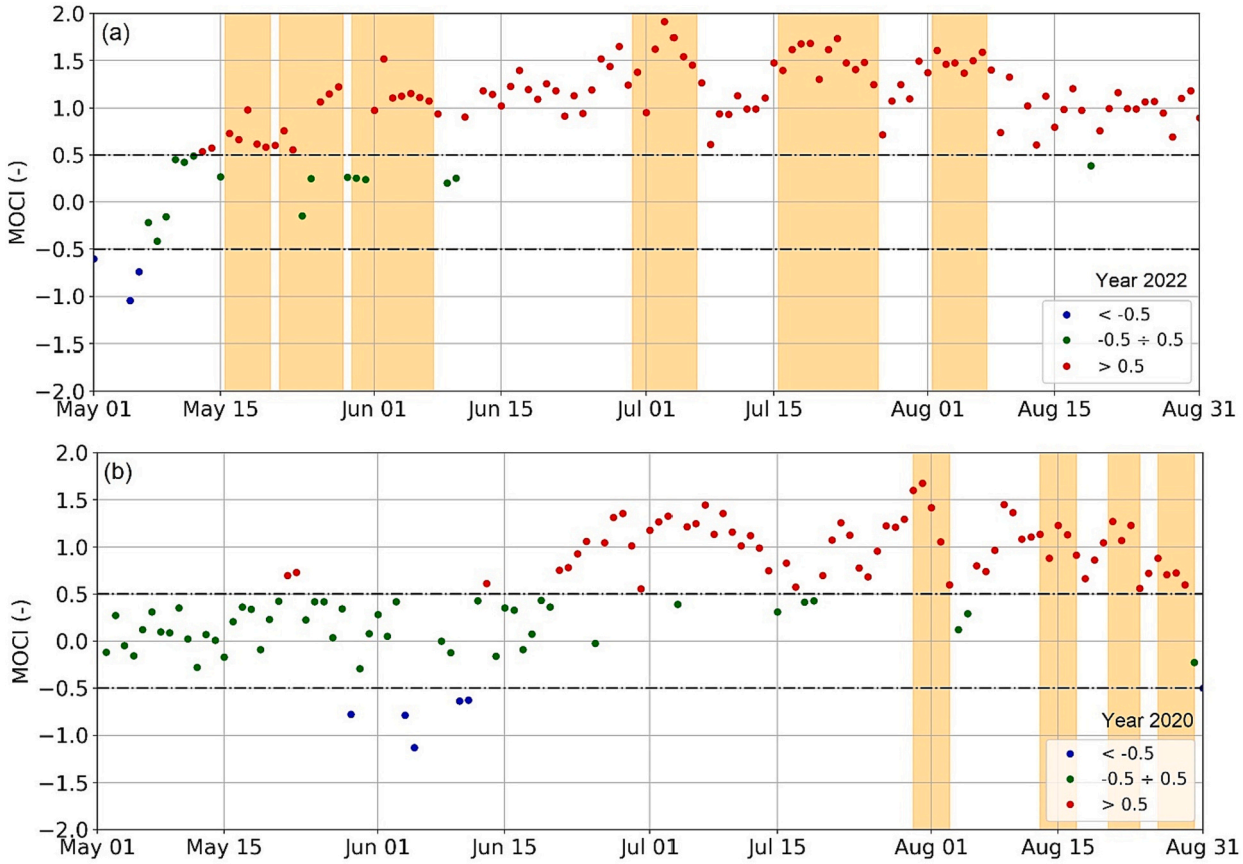

Fig. 7. Time series of daily maximum MOCI index for 2022 (panel a) and 2020 (panel b) at SAP station, showing cold (blue dots), neutral (green dots), and hot (red dots) sensations. The dash-dotted black lines depict the discomfort/comfort threshold values. Orange vertical bands depict the heatwaves. (For interpretation of the references to colour in this figure legend, the reader is referred to the web version of this article.)

equally affects sea and land, without significant impact on the offshore/inland pressure difference giving rise to the sea breeze (Stéfanon et al., 2014).

5.2. *Urban Heat Island Intensity*

The UHII is computed in the present study adopting the simplest definition of UHI, i.e., considering only two stations, located respectively in the urban centre and in the neighbouring rural area. Although the sites were chosen following the criteria proposed by Possega et al. (2022) (see Section 3.3), it should be noted that this definition does not allow to assess the spatial UHI inhomogeneity. Cecilia et al. (2023) performed a detailed evaluation of the UHI in Rome considering several in-situ meteorological stations, linking the UHII to satellite measurements of imperviousness, which describes the presence of artificially sealed surface. They found that, during the warm season, the northwest inland portion of Rome is typically characterised by daily averaged air temperatures in line with those of the urban centre and by daily maximum temperatures higher than in downtown Rome, in agreement with the results of the present study. This suggests that the correct choice of SAP and PAL sites for UHII evaluation.

Although the UHI is well evident from the time series of air temperatures (Fig. 5a and c), no synergy between the UHII and the heatwaves can be evinced by the daily-averaged UHII values, as also stated by Cecilia et al. (2023) for the same area. For this reason, it is crucial to deepen the analysis, not considering only the daily-averaged values but also examining the temporal evolution of the UHII to appreciate the day/night dissimilarities and above all, the amplification of the nocturnal UHI due to the heatwaves. This agrees with Founda et al. (2015), who detected an increase of UHII during summer night-time due to the heatwaves, with Possega et al. (2022), who found an intensification of nocturnal UHII in several European cities, and with Zinzi et al. (2020), who investigated the synergic effect of heatwaves and UHI in Rome over the period 2015–2017. Considering in-situ stations located in areas with different degree of urbanization, Zinzi et al. (2020) found an average UHII of 2.4 °C, which increases during heatwaves by 0.9 °C, compared to the rest of the season. Anyhow, for Zinzi et al. (2020) a heatwave occurs when the maximum apparent temperature is above the 75-99th percentiles for at least three days, i.e., they used constraints only partially comparable with those of the present study.

The outcomes presented here, together with those of other studies conducted around the world (e.g., see the review by Kong et al., 2021), suggest that the analysis of the heatwave/UHII interaction is not straightforward, since, although heatwaves can affect entire

regions, the final effect depends on the superimposition of several factors, not only linked to local temperature conditions but also - and above all - to the heatwave definition, geography (orography, distance from the coast or the reliefs, size of the urban area), and local background climate (Ramamurthy and Bou-Zeid, 2017).

One of the key factors in the interpretation of the outcomes is undoubtedly linked to the subjectivity of the heatwave definition: depending on the procedure chosen for the identification of the single heatwave event (e.g., temperature thresholds and duration), some days may be included/excluded from the study, significantly influencing the results. It suggests that is not possible to generalize the conclusions of a study to all the geographical and climatic areas, as pointed out by other authors (Ramamurthy and Bou-Zeid, 2017; Oliveira et al., 2021) and, thus, also the UHI adaptation and mitigation strategies must be defined considering local features.

5.3. Mediterranean outdoor comfort index

The MOCI time series highlight the exceptional thermal and thermo-hygrometric stress conditions occurred during summer 2022 when, unlike 2020, the overheating began at mid-May, continuing for most of the summer, without giving the possibility of recovery for the body and the environment.

The outcomes clearly prove that the detection of a heatwave - based on air temperature only - is not an effective metric for identifying thermo-hygrometric stress conditions, which in the warmest months can also occur in no-HW cases. In fact, the MOCI depends on other variables besides the temperature and has an absolute threshold for discomfort conditions (i.e., 0.5), while the heatwaves are based on relative thresholds (i.e., exceedances of percentiles with respect to a reference dataset). At the same time, the fact that during a single heatwave the maximum daily value of MOCI does not exceed the discomfort threshold is not indicative in terms of damage to the human health since, as demonstrated by Falasca et al. (2023), also the cumulative discomfort conditions due to the summer "thermo-hygrometric load" strains the human body and must be examined.

6. Conclusions

In this study, a comprehensive evaluation of the possible interactions between the extreme heat events and the main aspects of life in an urban environment has been conducted.

The main outcomes reveal that:

- the high temperatures measured in May and June 2022 suggest that the beginning of the summer season is increasingly anticipated and that further analyses are needed from the perspective of climate change in the Mediterranean basin (Founda et al., 2022);
- the heatwaves do not significantly influence the development of the sea breeze in terms of onset time, duration, and intensity. Only the cooling effect is favoured during the heatwaves (5.2 °C and 4.4 °C for HW and no-HW days in 2022, respectively);
- there is no appreciable synergy between the heatwaves and the daily-averaged UHII, which has a variation between the HW and no-HW sub datasets of 0.2 °C and 0.5 °C in 2022 and 2020, respectively;
- differences between diurnal and nocturnal UHII are observable. During night-time, the UHII is higher in HW than in no-HW days, further demonstrating the urban heating compared to the rural areas, while during daytime the temperature difference between urban and rural environments is lower;
- a heatwave does not necessarily involve thermo-hygrometric stress since the latter depends on several weather variables. Nonetheless, during the heatwaves, daily maxima of MOCI are higher when associated to high temperature as in July and August.

The findings expand our awareness of heatwaves variability and suggest the impossibility of a global generalisation of the scientific outcomes concerning the interaction between heatwaves, UHII, atmospheric dynamics, and thermo-hygrometric wellbeing. In fact, this synergy depends on the coexistence and mutual interaction of site-specific forcings such as orography, and geographical position. Moreover, the study of synoptic and local atmospheric dynamics and soil-moisture deficit are certainly some of the most important aspects for understanding the physical mechanisms driving extreme events and, therefore, planning tailored adaptation strategies. Given the importance of the issue, a univocal and globally applicable definition of heatwave which allows for the comparison of scientific results in different climatic zones is becoming increasingly important. Finally, the complexity of the phenomenon investigated, also read in the framework of climate change and, therefore, of continuous mutation, recommends the necessity for further investigations and it should be a warning for policymakers and government agencies to assess and design climate change mitigation and adaptation strategies also considering regional key factors, often overlooked.

Funding

This research was supported by BAQUNIN Project team, funded by ESA through the contract ID 4000126749/19/I-NS. Serena Falasca was funded by MUR (Ministero dell'Università e della Ricerca of Italy) under PON "Ricerca e Innovazione" 2014–2020 (D.M. 1062/2021).

CRediT authorship contribution statement

Annalisa Di Bernardino: Conceptualization, Software, Validation, Formal analysis, Investigation, Resources, Data curation, Writing – original draft, Writing – review & editing, Visualization. **Serena Falasca:** Conceptualization, Methodology, Software,

Writing – review & editing. **Anna Maria Iannarelli:** Methodology, Writing – review & editing. **Stefano Casadio:** Methodology, Writing – review & editing, Supervision, Funding acquisition. **Anna Maria Siani:** Methodology, Writing – review & editing, Supervision, Project administration.

Declaration of Competing Interest

The authors declare the following financial interests/personal relationships which may be considered as potential competing interests: Stefano Casadio reports financial support was provided by European Space Agency.

Data availability

The datasets analysed during the current study can be request to BAQUNIN, Osservatorio Milano Duomo Foundation, ARSIAL, ENAV, and CREA.

Acknowledgments

The authors gratefully acknowledge Osservatorio Milano Duomo Foundation for providing observations of the ClimateNetwork® stations, ARSIAL for providing Palombara meteorological data, ENAV for making the Pratica di Mare meteorological data available for this work, and the Council for Agricultural Research and Analysis of Agricultural Economics—Historical Meteorological Archive of the ex-CMA, Collegio Romano Observatory in supplying meteorological data. The authors gratefully acknowledge the BAQUNIN team for providing atmospheric data and for the insight and expertise that greatly assisted this work.

Appendix A. Supplementary data

Supplementary data to this article can be found online at https://doi.org/10.1016/j.uclim.2023.101735.

References

ARSIAL, 2022. Available online. https://www.siarl-lazio.it/index.asp (last accessed on 04 October 2022).
ASHRAE Standard 55, 2013. Thermal Environmental Conditions for Human Occupancy.
BAQUNIN, 2023. Available online. https://www.baqunin.eu/ (last accessed on 17 January 2023).
Beck, H.E., Zimmermann, N.E., McVicar, T.R., Vergopolan, N., Berg, A., Wood, E.F., 2018. Present and future Köppen-Geiger climate classification maps at 1-km resolution. Sci. Data 5 (1), 1–12.
Cecilia, A., Casasanta, G., Petenko, I., Conidi, A., Argentini, S., 2023. Measuring the urban heat island of Rome through a dense weather station network and remote sensing imperviousness data. Urban Clim. 47, 101355.
Chew, L.W., Liu, X., Li, X.X., Norford, L.K., 2021. Interaction between heat wave and urban heat island: A case study in a tropical coastal city, Singapore. Atmos. Res. 247, 105134.
CNR-ISAC, 2023. Climate Monitoring for Italy. Available online. https://www.isac.cnr.it/climstor/ (last accessed on 17 May 2023).
Consiglio per la Ricerca in Agricoltura e l''Analisi dell''Economia Agraria, 2022. Available online: https://www.crea.gov.it/home (last accessed on 04 October 2022).
COPERNICUS, 2022. OBSERVER: A wrap-up of Europe's summer 2022 heatwave. Available on. https://www.copernicus.eu/en/news/news/observer-wrap-europes-summer-2022-heatwave.
Di Bernardino, A., Iannarelli, A.M., Casadio, S., Mevi, G., Campanelli, M., Casasanta, G., Cede, A., Tiefengraber, M., Siani, A.M., Cacciani, M., 2021. On the effect of sea breeze regime on aerosols and gases properties in the urban area of Rome, Italy. Urban Clim. 37, 100842.
Di Bernardino, A., Iannarelli, A.M., Diémoz, H., Casadio, S., Cacciani, M., Siani, A.M., 2022a. Analysis of two-decade meteorological and air quality trends in Rome (Italy). Theor. Appl. Climatol. 1–17.
Di Bernardino, A., Iannarelli, A.M., Casadio, S., Pisacane, G., Mevi, G., Cacciani, M., 2022b. Classification of synoptic and local-scale wind patterns using k-means clustering in a Tyrrhenian coastal area (Italy). Meteorol. Atmospheric Phys. 134 (2), 1–12.
Falasca, S., Di Bernardino, A., Salata, F., 2023. On the identification and characterization of outdoor thermo-hygrometric stress events. Urban Clim. (accepted).
Fischer, E.M., Schär, C., 2010. Consistent geographical patterns of changes in high-impact European heatwaves. Nat. Geosci. 3 (6), 398–403.
Fischer, E.M., Seneviratne, S.I., Vidale, P.L., Lüthi, D., Schär, C., 2007. Soil moisture–atmosphere interactions during the 2003 European summer heat wave. J. Clim. 20 (20), 5081–5099.
Fondazione Osservatorio Milano Duomo, 2022. Available online: https://www.fondazioneomd.it/ (last accessed on 04 October 2022).
Founda, D., Pierros, F., Petrakis, M., Zerefos, C., 2015. Interdecadal variations and trends of the Urban Heat Island in Athens (Greece) and its response to heat waves. Atmos. Res. 161, 1–13.
Founda, D., Katavoutas, G., Pierros, F., Mihalopoulos, N., 2022. The extreme heat wave of summer 2021 in Athens (Greece): cumulative heat and exposure to heat stress. Sustainability 14 (13), 7766.
Fratianni, S., Acquaotta, F., 2017. The climate of Italy. Landscapes and landforms of Italy, pp. 29–38.
Geirinhas, J.L., Trigo, R.M., Libonati, R., Coelho, C.A., Palmeira, A.C., 2018. Climatic and synoptic characterization of heat waves in Brazil. Int. J. Climatol. 38 (4), 1760–1776.
Gershunov, A., Guirguis, K., 2012. California heat waves in the present and future. Geophys. Res. Lett. 39 (18).
He, X., Wang, J., Feng, J., Yan, Z., Miao, S., Zhang, Y., Xia, J., 2020. Observational and modeling study of interactions between urban heat island and heatwave in Beijing. J. Clean. Prod. 247, 119169.
Heaviside, C., Cai, X.M., Vardoulakis, S., 2015. The effects of horizontal advection on the urban heat island in Birmingham and the West Midlands, United Kingdom during a heatwave. Q. J. R. Meteorol. Soc. 141 (689), 1429–1441.
Hertig, E., 2020. Health-relevant ground-level ozone and temperature events under future climate change using the example of Bavaria, Southern Germany. Air Qual. Atmos. Health 13 (4), 435–446.
Hirschi, M., Seneviratne, S.I., Alexandrov, V., Boberg, F., Boroneant, C., Christensen, O.B., Formayer, H., Orlowsky, B., Stepanek, P., 2011. Observational evidence for soil-moisture impact on hot extremes in southeastern Europe. Nat. Geosci. 4 (1), 17–21.

Ialongo, I., Casale, G.R., Siani, A.M., 2008. Comparison of total ozone and erythemal UV data from OMI with ground-based measurements at Rome station. Atmos. Chem. Phys. 8 (12), 3283–3289.
Iannarelli, A.M., Di Bernardino, A., Casadio, S., Bassani, C., Cacciani, M., Campanelli, M., Casasanta, G., Cadau, E., Diémoz, H., Mevi, G., Siani, A.M., Cardaci, M., Dehn, A., Goryl, P., 2022. The Boundary Layer Air Quality-Analysis Using Network of Instruments (BAQUNIN) Supersite for Atmospheric Research and Satellite Validation over Rome Area. Bull. Am. Meteorol. Soc. 103 (2), E599–E618.
Jiang, S., Lee, X., Wang, J., Wang, K., 2019. Amplified urban heat islands during heat wave periods. J. Geophys. Res. Atmos. 124 (14), 7797–7812.
Kong, J., Zhao, Y., Carmeliet, J., Lei, C., 2021. Urban heat island and its interaction with heatwaves: a review of studies on mesoscale. Sustainability 13 (19), 10923.
Lhotka, O., Kyselý, J., Farda, A., 2018. Climate change scenarios of heat waves in Central Europe and their uncertainties. Theor. Appl. Climatol. 131 (3), 1043–1054.
Li, D., Bou-Zeid, E., 2013. Synergistic interactions between urban heat islands and heat waves: the impact in cities is larger than the sum of its parts. J. Appl. Meteorol. Climatol. 52 (9), 2051–2064.
Lionello, P., Scarascia, L., 2018. The relation between climate change in the Mediterranean region and global warming. Reg. Environ. Chang. 18 (5), 1481–1493.
Lorenzo, N., Díaz-Poso, A., Royé, D., 2021. Heatwave intensity on the Iberian Peninsula: future climate projections. Atmos. Res. 258, 105655.
Martin-Vide, J., Sarricolea, P., Moreno-García, M.C., 2015. On the definition of urban heat island intensity: the “rural” reference. Front. Earth Sci. 3, 24.
Oke, T.R., 1982. The energetic basis of the urban heat island. Q. J. R. Meteorol. Soc. 108 (455), 1–24.
Oliveira, A., Lopes, A., Correia, E., Niza, S., Soares, A., 2021. Heatwaves and summer urban heat islands: a daily cycle approach to unveil the urban thermal signal changes in Lisbon, Portugal. Atmosphere 12 (3), 292.
Ordóñez, C., Elguindi, N., Stein, O., Huijnen, V., Flemming, J., Inness, A., Flentje, H., Katragkou, E., Moinat, P., Peuch, V.-H., Segers, A., Thouret, V., Athier, G., van Weele, M., Zerefos, C.S., Cammas, J.-P., Schultz, M.G., 2010. Global model simulations of air pollution during the 2003 European heat wave. Atmos. Chem. Phys. 10 (2), 789–815.
Ortiz, L.E., González, J.E., Lin, W., 2018a. Climate change impacts on peak building cooling energy demand in a coastal megacity. Environ. Res. Lett. 13 (9), 094008.
Ortiz, L.E., Gonzalez, J.E., Wu, W., Schoonen, M., Tongue, J., Bornstein, R., 2018b. New York City impacts on a regional heat wave. J. Appl. Meteorol. Climatol. 57 (4), 837–851.
Papanastasiou, D.K., Melas, D., Bartzanas, T., Kittas, C., 2010. Temperature, comfort and pollution levels during heat waves and the role of sea breeze. Int. J. Biometeorol. 54 (3), 307–317.
Pérez, I., García, M.A., 2023. Climate change in the Iberian Peninsula by weather types and temperature. Atmos. Res. 284.
Perkins, S.E., 2015. A review on the scientific understanding of heatwaves—their measurement, driving mechanisms, and changes at the global scale. Atmos. Res. 164, 242–267.
Petenko, I., Mastrantonio, G., Viola, A., Argentini, S., Coniglio, L., Monti, P., Leuzzi, G., 2011. Local circulation diurnal patterns and their relationship with large-scale flows in a coastal area of the Tyrrhenian Sea. Bound.-Layer Meteorol. 139 (2), 353–366.
Pörtner, H.O., Roberts, D.C., Adams, H., Adler, C., Aldunce, P., Ali, E., Begum, R.A., Betts, R., Kerr, R.B., Biesbroek, R., Birkmann, J., Bowen, K., Castellanos, E., Cissé, G., Constable, A., Cramer, W., Dodman, D., Eriksen, S.H., Fischlin, A., Garschagen, M., Glavovic, B., Gilmore, E., Haasnoot, M., Harper, S., Hasegawa, T., Hayward, B., Hirabayashi, Y., Howden, M., Kalaba, K., Kiessling, W., Lasco, R., Lawrence, J., Lemos, M.F., Lempert, R., Ley, D., Lissner, T., Lluch-Cota, S., Loeschke, S., Lucatello, S., Luo, Y., Mackey, B., Maharaj, S., Mendez, C., Mintenbeck, K., Möller, V., Vale, M.M., Morecroft, M.D., Mukherji, A., Mycoo, M., Mustonen, T., Nalau, J., Okem, A., Ometto, J.P., Parmesan, C., Pelling, M., Pinho, P., Poloczanska, E., Racault, M.-F., Reckien, D., Pereira, J., Revi, A., Rose, S., Sanchez-Rodriguez, R., Schipper, E.L.F., Schmidt, D., Schoeman, D., Shaw, R., Singh, C., Solecki, W., Stringer, L., Thomas, A., Totin, E., Trisos, C., van Aalst, M., Viner, D., Wairiu, M., Warren, R., Yanda, P., Ibrahim, Z.Z., Adrian, R., Craig, M., Degvold, F., Ebi, K.L., Frieler, K., Jamshed, A., McMillan, J., Mechler, R., New, M., Simpson, N.P., Stevens, N., 2022. Climate Change 2022: Impacts, Adaptation, and Vulnerability. In: Contribution of Working Group II to the Sixth Assessment Report of the Intergovernmental Panel on Climate. Intergovernmental Panel on Climate Change (IPCC), Change, Geneva, 36 p.
Possega, M., Aragão, L., Ruggieri, P., Santo, M.A., Di Sabatino, S., 2022. Observational evidence of intensified nocturnal urban heat island during heatwaves in European cities. Environ. Res. Lett. 17 (12), 124013.
Ramamurthy, P., Bou-Zeid, E., 2017. Heatwaves and urban heat islands: a comparative analysis of multiple cities. J. Geophys. Res. Atmos. 122 (1), 168–178.
Richard, Y., Pohl, B., Rega, M., Pergaud, J., Thévenin, T., Emery, J., Dudek, J., Vairet, T., Zito, S., Chateau-Smith, C., 2021. Is Urban Heat Island intensity higher during hot spells and heat waves (Dijon, France, 2014–2019)? Urban Clim. 35, 100747.
Salata, F., Golasi, I., de Lieto Vollaro, R., de Lieto Vollaro, A., 2016. Outdoor thermal comfort in the Mediterranean area. A transversal study in Rome, Italy. Build. Environ. 96, 46–61.
Satyanarayana, G.C.H., Rao, D.V.B., 2020. Phenology of heat waves over India. Atmos. Res. 105078.
Simpson, J.E., 1994. Sea Breeze and Local Winds. Cambridge University Press.
Stéfanon, M., D'Andrea, F., Drobinski, P., 2012. Heatwave classification over Europe and the Mediterranean region. Environ. Res. Lett. 7 (1), 014023.
Stéfanon, M., Drobinski, P., D'Andrea, F., Lebeaupin-Brossier, C., Bastin, S., 2014. Soil moisture-temperature feedbacks at meso-scale during summer heat waves over Western Europe. Clim. Dyn. 42 (5), 1309–1324.
Stewart, I.D., 2011. A systematic review and scientific critique of methodology in modern urban heat island literature. Int. J. Climatol. 31 (2), 200–217.
Tomlinson, C.J., Chapman, L., Thornes, J.E., Baker, C.J., 2012. Derivation of Birmingham's summer surface urban heat island from MODIS satellite images. Int. J. Climatol. 32 (2), 214–224.
UN, 2018. The World Urbanization Prospects: The 2018 Revision. The United Nations, New York. http://esa.un.org/UNPOP/wup/index.htm. accessed on 04 August 2022.
Vanderplanken, K., van den Hazel, P., Marx, M., Shams, A.Z., Guha-Sapir, D., van Loenhout, J.A.F., 2021. Governing heatwaves in Europe: comparing health policy and practices to better understand roles, responsibilities and collaboration. Health Res. Policy Syst. 19 (1), 1–14.
Ward, K., Lauf, S., Kleinschmit, B., Endlicher, W., 2016. Heat waves and urban heat islands in Europe: A review of relevant drivers. Sci. Total Environ. 569, 527–539.
WMO, 2022. Available online: https://public.wmo.int/en/media/news/wmo-has-no-immediate-plans-name-heatwaves#:%E2%88%BC:text=A%20heat%20wave%20is%20broadly,and%20declare%20a%20heat%20wave (last accessed on 27 January 2023).
Xu, Z., FitzGerald, G., Guo, Y., Jalaludin, B., Tong, S., 2016. Impact of heatwave on mortality under different heatwave definitions: a systematic review and meta-analysis. Environ. Int. 89, 193–203.
Xu, P., Wang, L., Huang, P., Chen, W., 2021. Disentangling dynamical and thermodynamical contributions to the record-breaking heatwave over Central Europe in June 2019. Atmos. Res. 252, 105446.
Zhao, L., Lee, X., Smith, R.B., Oleson, K., 2014. Strong contributions of local background climate to urban heat islands. Nature 511 (7508), 216–219.
Zhou, B., Rybski, D., Kropp, J.P., 2013. On the statistics of urban heat island intensity. Geophys. Res. Lett. 40 (20), 5486–5491.
Zhou, X., Carmeliet, J., Sulzer, M., Derome, D., 2020. Energy-efficient mitigation measures for improving indoor thermal comfort during heat waves. Appl. Energy 278, 115620.
Zinzi, M., Agnoli, S., Burattini, C., Mattoni, B., 2020. On the thermal response of buildings under the synergic effect of heat waves and urban heat island. Sol. Energy 211, 1270–1282.